PROCEEDINGS OF SPIE

SPIEDigitalLibrary.org/conference-proceedings-of-spie

Optical magnetic field sensor based on guided-mode resonance with Ni subwavelength grating/waveguide structure

Yuusuke Takashima, Masanobu Haraguchi, Yoshiki Naoi

Yuusuke Takashima, Masanobu Haraguchi, Yoshiki Naoi, "Optical magnetic field sensor based on guided-mode resonance with Ni subwavelength grating/waveguide structure," Proc. SPIE 10928, High Contrast Metastructures VIII, 109281S (4 March 2019); doi: 10.1117/12.2509490

SPIE.

Event: SPIE OPTO, 2019, San Francisco, California, United States

Optical magnetic field sensor based on guided-mode resonance with Ni subwavelength grating/waveguide structure

Yuusuke Takashima*[a], Masanobu Haraguchi[a], Yoshiki Naoi[a]
[a] Graduate School of Technology and Science, Tokushima University, 2-1 Minami-josanjima, Tokushima, Japan 770-8506

ABSTRACT

Highly sensitive optical sensor for magnetic field detection was experimentally demonstrated using a guided-mode resonance in waveguide with Ni nano-grating. The electromagnetic field distribution was calculated by finite-difference time-domain method in order to estimate the sensing performance of our device. The calculation results indicated that the optical characteristics of our sensor considerably varied with applying magnetic field. We fabricated the Ni-subwavelength grating/ Si_3N_4 waveguide structure on the optical glass substrate using electron beam lithography technique. The reflection peak resulting from the guided-mode in the waveguide was obtained with normal incident geometry. The peak intensity depended on static magnetic field applied to the structure, and the intensity changed by about 5 % for the magnetic field intensity of 39.4 mT. These experimental results suggest our sensor can sensitively detect magnetic field while avoiding use of the complex and expensive system, and our device is pretty suitable for the integration devices in internet of things society.

Keywords: magnetic field sensor, subwavelength grating, waveguide, guided-mode,

1. INTRODUCTION

In internet of things (IoT) society, sensing devices are important and essential techniques. In particular, magnetic field sensing is one of the most important technique in various fields, such as industry, chemical, and medical science. The use of the magnetic field sensor in the harsh environment leads to new applications, for example position control of robot working in radioactive environment. In order to achieve the applications, magnetic field sensor with high sensitivity, withstand for the environment, and portable device size are highly desirable.

The Hall and giant-magneto-resistive (GMR) elements, which convert the magnetic field to current or voltage, are widely commercialized and used for the highly sensitive magnetic field sensing[1-5]. However, the sensitivity of these elements are considerable influenced by electromagnetic interference. To achieve extreme high sensitivity, superconducting-quantum-interference-devices (SQUIDs) have been developed[6, 7]. Although the sensitivities of SQUIDs reach to a few fT order, the system setups are very large and cumbersome. Such system considerably restricts the practical use of SQUIDs. Several groups have reported optical sensors with magnetic fluid, such as Bragg fiber[8,9], photonic-crystal fiber[10,11], and interferometer[12,13], because the sensors have the several advantages of rapid response-speed, compactness, and immunities for the electromagnetic interferences. However, expensive setup and the specialized techniques of the measurement systems still be required.

In this paper, we theoretically and experimentally demonstrated highly sensitive magnetic field sensor with very simple system by using ferromagnetic subwavelength grating (SWG)/waveguide structure. The electromagnetic field distribution was calculated by finite-difference time-domain method in order to estimate the sensing performance of our device. The calculated electromagnetic field indicated that the excitation conditions of the guided-mode in the waveguide was significantly modified with the magnetization of the ferromagnetic SWG. We also fabricated the SWG/waveguide structure using electron beam lithography techniques. The experimental reflection peak associated with the guided-mode was obtained. The intensity of the reflection peak varied with applying the external magnetic field, and the minuscule magnetic field was measured with very simple normal incident system.

*takashima@ee.tokushima-u. ac.jp; phone +81-88-656-7447; fax +81-88-656-7447

High Contrast Metastructures VIII, edited by Connie J. Chang-Hasnain, Andrei Faraon, Weimin Zhou, Proc. of SPIE Vol. 10928, 109281S · © 2019 SPIE
CCC code: 0277-786X/19/$18 · doi: 10.1117/12.2509490

2. DESGIN OF SWG/WAVEGUIDE FOR MAGNETIC SENSING

In this section, we explain the operating mechanism and design of our sensor. Figure 1 shows the schematic structure of our magnetic field sensor. As shown in Fig. 1, ferromagnetic material-based SWG is placed on the waveguide structure, which is composed of substrate and core layer.

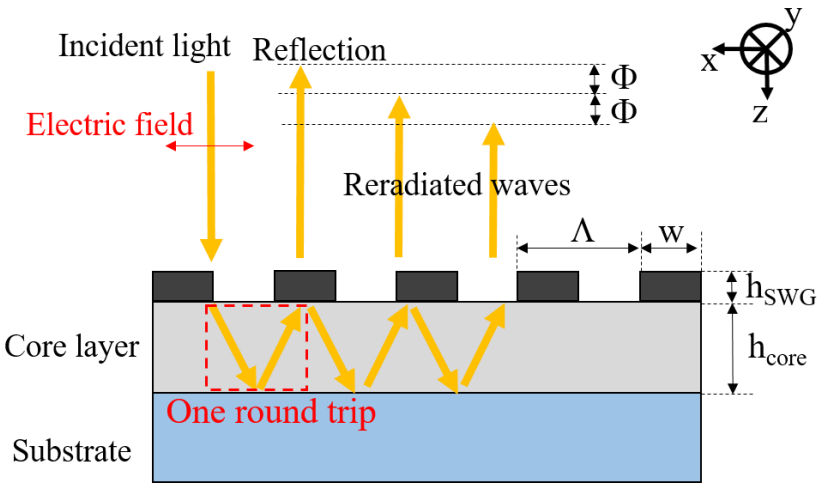

Figure 1. Sensing mechanism of our magnetic sensor using SWG/waveguide structure. The square region surrounded by red dashed lines denotes the one round trip of the guided-mode in core layer.

The grating period, grating bar width, grating thickness, and core thickness correspond to the symbols Λ, w, h_{SWG}, and h_{core}, respectively. The material covering the structure is air. We consider the normal incidence of p-polarized plane wave to the structure. The electric field of the p-polarized light is perpendicular to the grating bars (denote red arrow in Fig. 1). The incident light is diffracted from SWG, whose period is shorter than the incident wavelength in free space (λ_0). All diffractions, except for the 0th order diffractions, are evanescent wave because of the large wavenumber modulation by SWG. The guided-mode can be excited in the core layer when the wavenumber of the mode matches to that of the diffractions. The excited guided-mode travels along the core layer with reflection at the core-substrate interface. The guided-mode retuned to the SWG is partially reradiated into the incident region by SWG. The rest is reflected at the SWG-core interface. The same phenomena occur at each times guided-mode enters the SWG. The phase retardation of the reradiated wave over one round trip (denote the red dashed region in Fig. 1) Φ is given by[14]

$$\Phi = 2k_{mode}h_{core} + \Phi_s + \Phi_{SWG} \tag{1}$$

and

$$k_{mode} = \frac{2\pi}{\lambda_0}\left(n_c^2 - n_{eff}\right)^{1/2}. \tag{2}$$

Where, the term of k_{mode} is z-direction wavenumber of the guided-mode. The term of n_{eff} for normal incidence is written by $n_{eff} = m\lambda_0/\Lambda$, and m is diffraction order. The covering material refractive index (n_c) is that of air. The terms of Φ_s and Φ_{SWG} represent phase changes owing to reflections at the core-substrate and the SWG-core interfaces, respectively. These phase changes are defined as follows[14].

$$\Phi_s = -2\tan\left[\left(\frac{n_{core}}{n_{sub}}\right)^{2\rho}\frac{\left|\left(n_{sub}^2-n_{eff}^2\right)^{1/2}\right|}{\left(n_{core}^2-n_{eff}^2\right)}\right]. \quad (3)$$

$$\Phi_{SWG} = -2\tan\left[\left(\frac{n_{core}}{n_{SWG}}\right)^{2\rho}\frac{\left|\left(n_{SWG}^2-n_{eff}^2\right)^{1/2}\right|}{\left(n_{core}^2-n_{eff}^2\right)}\right]. \quad (4)$$

The symbols n_{core} and n_{sub} are refractive indices of the core and the substrate, respectively. The n_{SWG} is effective refractive index of SWG. The ρ is 1 for p-polarization and is 0 for s-polarization (whose electric field is parallel to grating bars). If all reradiated light are in-phase (integer multiple of 2π) to the reflection (the 0th reflected diffraction), these waves form the constructive interference and reinforces each other. As a result, one finds the very sharp and strong peak in reflection spectra[15-19]. When the ferromagnetic SWG is magnetized by an external magnetic field, the movement of electric dipole in the SWG induced by the incident light is influenced by its magnetization. This induces the non-diagonal components of the dielectric tensor of the ferromagnetic material. As a result, the polarization state of the light is rotated at the transmission and reflection in the magnetized ferromagnetic material[20-22]. The phenomena are well known as Faraday- and Kerr-rotation. From Equations (1) to (4), the phases of the reradiated waves from the waveguide depend on the polarization state of light. Hence, the intensity of the reflection peak resulting from the interference between the reflection and reradiated waves varies with the applying magnetic field. According to the sensing mechanism explained above, we designed the SWG and the waveguide structure in order to obtain the reflection peak at the visible wavelength, owing to its ease of experimentation. The material of the waveguide core and the substrate are Si_3N_4 and glass substrate, respectively. Ni is also selected as the ferromagnetic SWG material because Ni nano-rod has very large saturation magnetization[23]. The refractive index values of Si_3N_4 and Ni were taken from these literatures[24, 25]. The structural parameters, such as grating period, grating bar width, core layer thickness are fixed to Λ = 400 nm, w = 200 nm, and h_{core} = 200 nm, respectively to coincide the wavenumber of the 1st order diffractions with that of guided-mode. The Ni-SWG thickness is set to 50 nm for avoiding the significant light absorption.

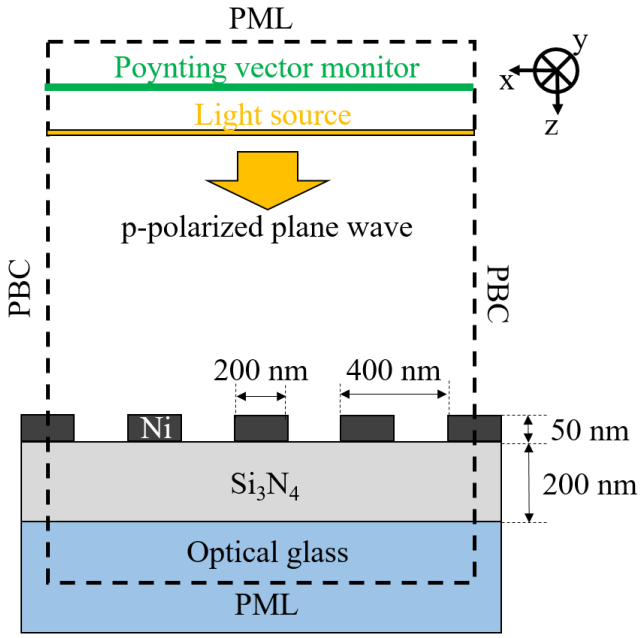

Figure 2. FDTD numerical calculation model of our sensor. The dashed lines indicates boundary conditions. The electromagnetic field distribution inside the boundaries was calculated.

We calculated the electromagnetic field distribution of the designed structure by FDTD numerical method to estimate the optical characteristics of the designed structure. The model for FDTD numerical calculation is shown in Fig. 2. The dashed lines indicate the boundary conditions, and the fields in the area surrounded by 4-boundaries were calculated. The periodic boundary condition (PBC), at which the electromagnetic field distribution infinitely repeats, was employed for x-direction. We also used 2-dimensional calculation, where the structural length along y-direction was infinite, because the actual grating length was large enough to apply the infinite assumption. We used perfect matched layer (PML) boundary condition for z-direction, and no reflection occurs at the PML boundaries. The intensity of light outside the PML boundaries rapidly deceased and had no effect on the field distribution inside the calculation area. The p-polarized plane wave from the light source vertically entered into the Ni-SWG/waveguide structure. The intensity of the reflected light from the structure was evaluated via Poyinting vector through the monitor, which was placed above the light source.

The magnetic sensing performance was also estimated in the calculation. The quantum physics is required for the precise behavior of the magnetic responses of the ferromagnetic material. Although we consider the equivalent change of Ni refractive index by the magnetic field because this assumption is adequate enough for rough and qualitative estimation of the sensing performance. We assume that free electron mainly contributes to Ni magnetic response. In the case of applying magnetic field to Ni, the refractive index (n_{Ni}) is given by classical physic model as follows[20].

$$n_{Ni}(\omega) = \sqrt{1 - \frac{nq^2}{m_e \epsilon_0} \frac{\omega^2 + i\omega\gamma}{(\omega^2 + i\gamma\omega)^2 - \omega^2\omega_c^2}}. \quad (5)$$

The symbols in Equation (5), the term of n, q, m_e, ε_0, and ω are the electron density, charge of the electron, effective electron mass, permittivity in vacuum, and angular frequency of the incident light, respectively. The damping factor is represented as γ. The symbol of ω_c is given as $\omega_c = qB/m_e$, and the symbol B denotes magnetic field value. Equation (5) means that the refractive index of Ni reduces with applying magnetic field. The decreasing of Ni refractive index by magnetic field (Δn_{Ni}) is defined as $\Delta n_{Ni} = n_{Ni}(B) - n_{Ni}(0)$, and the $n_{Ni}(B)$ and $n_{Ni}(0)$ are the refractive index value of Ni with and without magnetic field.

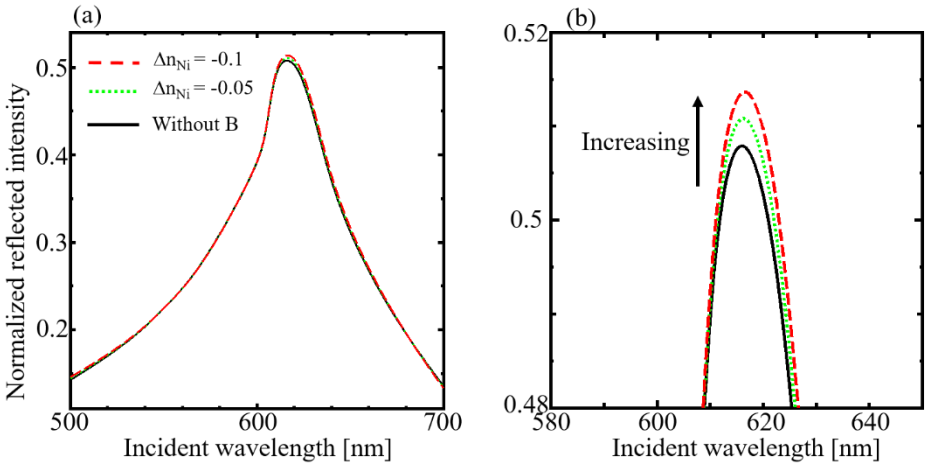

Figure 3. (a) Calculated reflection spectra of the Ni-SWG/waveguide. (b) Enlarged view of Fig. 3 (a) around the peak wavelength of 620 nm. The intensities were evaluated via Poynting vector and were normalized by that of the incident light.

The calculated reflection spectra are shown in Fig. 3 (a) and (b) as a function of the incident wavelength. Figure 3 (b) shows the enlarged view of Fig. 3 (a) around the wavelength of 620 nm. In Fig. 3 (a), and (b), the reflection peak is found around the wavelength of 620 nm, and the reflection peak intensity increases when the refractive index of Ni equivalently decreases by the magnetic field. We also show x- and z-components of the electric field distribution at the peak wavelength in Fig. 4 (a) and (b), respectively. The field amplitudes are normalized by that of the incident light. As shown in Fig. 4 (a), the wavefront of the diffracted light is distorted. The distribution indicates the wavenumber of the incident light is

modulated for x-direction via Ni-SWG. In Fig. 4(b), no z-component of the electric field is in the incident region and means that the only 0th diffraction order propagates outside the SWG/waveguide structure. In Fig. 4(b), in contrast, one finds the z-component of the electric field around the waveguide core region, regardless of the z-direction incidence. The electric field is concentrated at the interference between the core and the substrate. This indicates that the diffractions couple with the guided-mode, which propagates along x-direction. Thus, we can attribute the reflection peak in Fig. 3 to excitation of the waveguide mode, and these calculation results show that our sensor can detect magnetic field with very simple vertical incidence system.

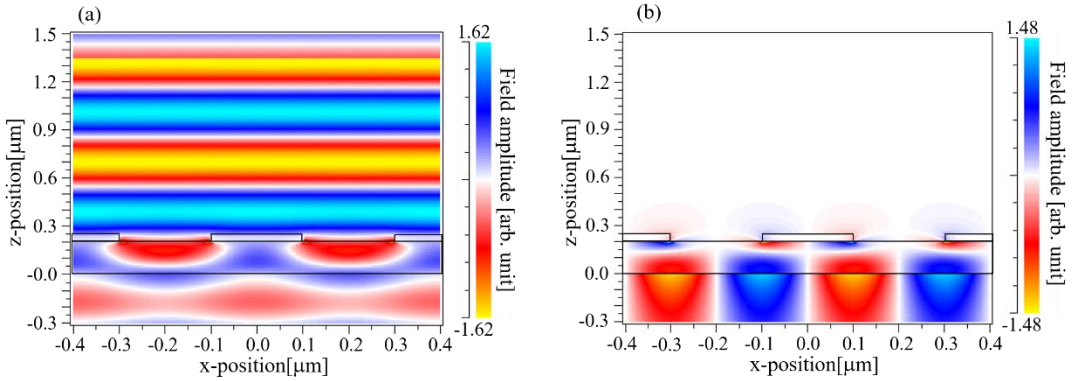

Figure 4. Calculated electric field distribution around the Ni-SWG/waveguide structure. (a) x-component (b) z-component at the reflection peak wavelength. The field amplitudes was normalized by that of the incident wave.

3. EXPERIMENTAL RESULTS AND DISCUSSION

We explain the fabrication process of the designed structure by using electron beam lithography techniques. At first, A 200 nm thickness of the Si_3N_4 was chemically deposited on the glass substrate (Multiple purpose D263 T eco Thin Glass: SCHOTT). EB resist (ZEP-520A: Zeon) film with about 100 nm thickness was spin-coated on the Si_3N_4 film. The grating pattern was formed by EB lithography, and the pattern was developed by dimethyl-sulfoxide at 80 °C. A 50 nm Ni film was evaporated on the nano-patterned resist grating. Figure 5 shows scanning electron microscope (SEM) image of the fabricated sample surface. The fabricated Ni-SWG has 400 nm period and 200 nm grating width, and the whole sample area size is 300 x 300 μm^2.

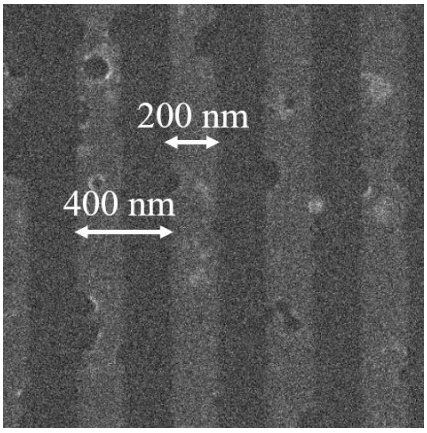

Figure 5. SEM image of the fabricated Ni-SWG/waveguide structure.

The magnetic response for the fabricated sample was measured. The experimental set up is as follows. A halogen lamp was used as a visible light source. A planer-convex lens was placed in the front of the halogen lamp to collimate the light from the lamp. A polarization state of the collimated light was p-polarized by polarizer. The p-polarized light was focused and normally entered in the sample area by focusing lens (x 20: NA = 0.46). The reflected light from the sample was measured by spectrometer (Ocean optics USB 4000). The sample is also placed on the top of the solenoid coil, and the static magnetic field (B) was vertically applied to the sample. The magnetic field value was monitored using Gauss meter (Lake Shore 410).

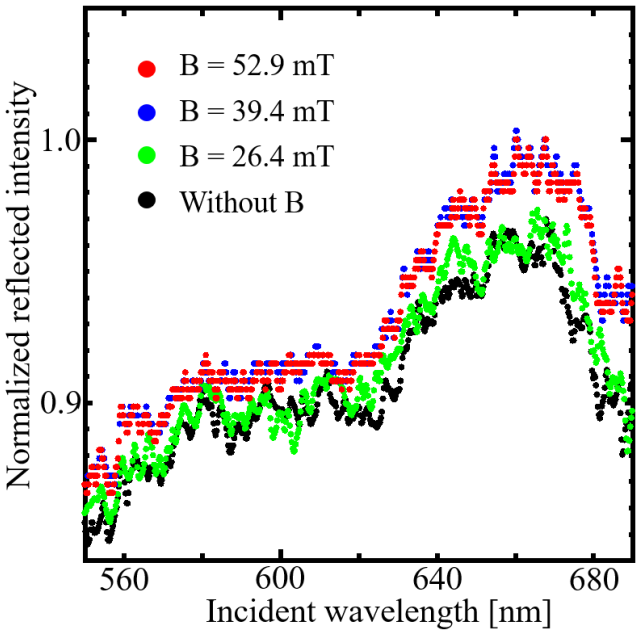

Figure 6. Dependence of the reflection spectra of the fabricated sample on the magnetic field B. The direction of the magnetic field was vertical for the sample surface.

Figure 6 shows the dependence of the normalized reflection spectra of the fabricated sample on the applied static magnetic field value. At the wavelength of 675 nm, we obtain the reflection peak, which was resulting from the guided-mode in core layer. The reflection peak intensity increases with the increasing applied magnetic field value, while the intensities at other wavelengths shows no considerable intensity changes. The tendency of the experimental result shows good agreement with the theoretical prediction by FDTD method. The peak intensity nonlinearly increased with applying magnetic field up to 39.4 mT, and the intensity change was saturated when the magnetic field of 52.9 mT was applied. We consider that the origin of nonlinear intensity change and saturation is magnetic hysteresis characteristics of Ni-SWG[23]. The intensity increasing in the range from B = 0 to B = 39.4 mT reaches to about 5 % of the peak intensity without magnetic field, and this sensitivity corresponds to comparable sensitivity of other devices on literatures[8, 9, 26]. The origin of such high sensitivity can be attributed to the accumulation of polarization rotation by the magnetized SWG. The excited guided-mode propagates along core layer with reflection at SWG-core and core-substrate interfaces. The mode polarization state is rotated via the reflection at the magnetized SWG-core interface. The rotation is accumulated for each reflection at SWG-core. Thus, the interference condition between the 0th order diffraction and reradiated waves from the waveguide is significantly modified by the magnetic field, and the very high sensitivity can be obtained. These experimental results indicate that our sensor sensitively measure magnetic field without complex and specialized system, and these advantages will be suitable for request for the integration devices in IoT society.

4. SUMMARY

In summary, the magnetic field sensor with very simple normal incidence was experimentally realized using Ni-SWG/waveguide structure. The Ni-SWG and Si_3N_4 waveguide structure were designed using wavenumber matching condition of the guided-mode. To estimate the sensing performance of our sensor, we calculated the electromagnetic field distribution in the structure using FDTD numerical method. The theoretical results indicates that the intensity of the reflection peak resulting from the guided-mode increases with the application of external magnetic field, and our sensor measures the magnetic field without complex system. The measured intensity changes of the reflection peak was nearly 5% with applying magnetic field of 39.4 mT. These results suggest that our sensor will play important role in the integration devices.

ACKNOWLEDGEMENTS

This work is partially supported by JSPS KAKENHI Grant Number JP18K04238 and LED general platform project of Tokushima University.

REFERENCES

[1] Besse, P. A., Boero, G., Demierre, M., Pott, V. and Popovic R., "Detection of a single magnetic microbead using a miniaturized silicon Hall sensor," Appl. Phys. Lett. 80(22), 4199-4201 (2002).
[2] Ejsing, L., Hansen, M. F., Menon, A. K., Ferreira, H. A., Graham, D. L. and Freitas P. P., "Planar Hall effect sensor for magnetic micro- and nanobead detection," Appl. Phys. Lett. 84(23), 4729-4731 (2004).
[3] Sharon, Y., Khachatryan, B. and Cheskis, D., "Toward a low current Hall effect sensor," Sens. Actuators A 279, 278-283 (2018).
[4] Pannetier, M., Fermon, C., Goff, G. L., Simola, J. and Kerr, E. "Femtotesla magnetic field measurement with magnetoresistive sensors," Science 304(5677), 1648-1650 (2004).
[5] Reig, C., Cubells-Beltrán, M. D. and Muñoz, D. R., "Magnetic field sensors based on Giant Magnetoresistance (GMR) technology: Applications in electrical current sensing," Sensors 9(10), 7919-7942 (2009).
[6] Barthelmess, H. J., Halverscheid, M., Schiefenhovel, B., Heim, E., Schilling, M. and Zimmermann, R., "Low-noise biomagnetic measurements with a multichannel dc-SQUID system at 77 K," IEEE Trans. Appl. Superconduct. 11(1), 657-660 (2001).
[7] Gallop, J., "SQUIDs: some limits to measurement," Supercond. Sci. Technol. 16(12), 1575-1582 (2003).
[8] Dai, J., Yang, M., Li, X., Liu, H. and Tong, X., "Magnetic field sensor based on magnetic fluid clad etched fiber Bragg grating," Opt. Fiber Technol. 17(3), 210-213 (2011).
[9] Yang, D., Du, L., Xu, Z., Jiang, Y., Xu, J., Wang, M., Bai, Y. and Wang, H., "Magnetic field sensing based on tilted fiber Bragg grating coated with nanoparticle magnetic fluid," Appl. Phys. Lett. 104(6), 061903 (2014).
[10] Thakur, H. V., Nalawade, S. M., Gupta S., Kitture, R. and Kale, S. N., "Photonic crystal fiber injected with Fe_3O_4 nanofluid for magnetic field detection," Appl. Phys. Lett. 99(16), 161101 (2011).
[11] Zu, P., Chan, C. C., Gong, T., Jin, Y., Wong, W. C. and Dong, X., "Magneto-optical fiber sensor based on bandgap effect of photonic crystal fiber infiltrated with magnetic fluid," Appl. Phys. Lett. 101(24), 241118 (2012).
[12] Oh, K. D., Wang, A. and Glaus, R. O., "Fiber-optic extrinsic Fabry-Perot dc magnetic field sensor," Opt. Lett. 29(18), 2115-2117 (2004).
[13] Li, Z., Liao, C., Song, J., Wang, Y., Zhu, F., Wang, Y. and Dong, X., "Ultrasensitive magnetic field sensor based on an in-fiber Mach-Zehnder interferometer with a magnetic fluid component," Photon. Res. 4(5), 197-201 (2016).
[14] Sahoo, P. K., Sarkar, S. and Joseph, J., "High sensitive guided-mode-resonance optical sensor employing phase detection," Sci. Rep. 7, 7607 (2017).
[15] Liu, Z. S., Tibuleac, S., Shin, D., Young, P. P. and Magnusson R., "High-efficiency guided-mode resonance filter," Opt. Lett. 23(19), 1556-1558 (1998).
[16] Wang, Z., Sang, T., Wang, L., Zhu, J., Wu, Y. and Chen, L., "Guided-mode resonance Brewster filters with multiple channels," Appl. Phys. Lett. 88(25), 251115 (2006).

[17] Kintaka, K., Majima, T., Inoue, J., Hatanaka, K., Nishii, J. and Ura, S., "Cavity-resonator-integrated guided-mode resonance filter for aperture miniaturization," Opt. Express 20(2), 1444-1449 (2012).
[18] Lee, K. J., Giese, J., Ajayi, L., Magnusson, R. and Johnson, E., "Resonant grating polarizers made with silicon nitride, titanium dioxide, and silicon: Design, fabrication, and characterization," Opt. Express 22(8), 9271-9281 (2014).
[19] Wu, S., Liu, B., Zhu, Z., Cheng, C., Chen, H., Gu, M., Chen, L., Liu, J., Ouyang, X., Xue, C. and Wu, Y., "Guided-mode resonance assisted directional emission of a wavelength-shifting film for application in scintillation detection," Opt. Express 24(1), 231-238 (2016).
[20] Dresselhaus, G., Kip, A. F. and Kittel, C., "Plasma resonance in crystals: observations and theory," Phys. Rev. 100(2), 618-625 (1955).
[21] Melle, S., Menéndez, J. L., Armelles, G., Navas, D., Vázquez, M., Nielsch, K., Wehrspohn, R. B. and Gösele, U., "Magneto-optical properties of nickel nanowire arrays," Appl. Phys. Lett. 83(22), 4547-4549 (2003).
[22] Khanikaev, A. B., Baryshev, A. V., Fedyanin, A. A., Granovsky, A. B. and Inoue, M., "Anomalous Faraday Effect of a system with extraordinary optical transmittance," Opt. Express 15(11), 6612-6622 (2007).
[23] Ferré, R., Ounadjela, K., George, J. M., Piraux, L. and Dubois, S., "Magnetization processes in nickel and cobalt electrodeposited nanowire," Phys. Rev. B 56(21), 14066-14075 (1997).
[24] Johnson, P. B. and Christy, R. W., "Optical constants of transition metals: Ti, V, Cr, Mn, Fe, Co, Ni, and Pd," Phys. Rev. B 9(12), 5056-5070 (1974).
[25] Luke, K., Okawachi, Y., Lamont, M. R. E., Gaeta, A. L. and Lipson, M., "Broadband mid-infrared frequency comb generation in a Si_3N_4 microresonator," Opt. Lett. 40(21), 4823-4826 (2015).
[26] Takashima, Y., Haraguchi, M. and Naoi, Y., "Highly sensitive magnetic field sensor with normal-incidence geometry using Ni-based bilayer subwavelength periodic structure operating in visible-wavelength region," Jpn. J. Appl. Phys. 57(8S2), 08PE01 (2018).